Morphology Effects on Nonisotropic Thermal Conduction of Aligned Single-Walled and Multi-Walled Carbon Nanotubes in Polymer Nanocomposites

Hai M. Duong,*,†,‡,§ Namiko Yamamoto,† Khoa Bui,|| Dimitrios V. Papavassiliou,|| Shigeo Maruyama,⊥ and Brian L. Wardle†

Department of Aeronautics and Astronautics, Massachusetts Institute of Technology, Cambridge, Massachusetts 02139, Department of Materials Science and Metallurgy, University of Cambridge, Cambridge CB2 3QZ, U.K., Department of Mechanical Engineering, National University of Singapore, Singapore 117576, Singapore, School of Chemical, Biological and Materials Engineering, The University of Oklahoma, Norman, Oklahoma 73019, and Department of Mechanical Engineering, The University of Tokyo, Bunkyo, Tokyo 113-8656, Japan

Received: March 9, 2010; Revised Manuscript Received: March 24, 2010

Carbon nanotube (CNT)−CNT contact and CNT distribution effects on anisotropic thermal transport in aligned CNT−polymer nanocomposites (PNCs) are studied using an off-lattice Monte Carlo numerical simulation. Inter-CNT contact and the associated thermal boundary resistance are shown here to significantly affect transport properties of PNCs, including anisotropy ratios. Previous studies have considered the effective thermal conductivities of CNT−PNCs using only a very large CNT−CNT thermal boundary resistance (TBR) compared to that of the CNT−matrix TBR as a limiting case. As CNT−CNT TBR is currently an unquantified parameter for CNT−polymer systems, and because it may be reduced by various techniques, heat transport with CNTs in contact is studied for a wide range of CNT−CNT TBR values, varying from 2 to 25 × 10^{-8} m^2 K/W. The degree of CNT−CNT contact, CNT spatial distribution, and CNT−CNT TBR relative to CNT−matrix TBR are considered for 1−20% volume fraction of aligned single-walled and multi-walled CNTs. When CNT−CNT contact is significant or CNT−CNT TBR is low (relative to the CNT−matrix TBR), then heat transport is dominated by CNT−CNT contact effects, rather than CNT−matrix interfacial effects. As an example, effective nanocomposite thermal conductivity parallel to the CNT axis is shown to increase by up to ∼4× due to CNT−CNT contact effects. A critical value of CNT−CNT TBR is identified that controls whether the addition of conductive CNTs in the insulating polymer increases or decreases thermal transport. These simulation results can be very useful for developing techniques to enhance the effective thermal conductivity of composites using conductive nanomaterials embedded in (polymer) matrices, and assist experimentalists in interpreting heat conduction measurements.

1. Introduction

Applications of carbon nanotubes (CNTs) vary from microscale thermal tapes and interface materials in electric circuits[1,2] to macroscale aerospace structural composites[3,4] that benefit also from lightweight and other multifunctional (mechanical and electrical) property enhancements due to the exceptional intrinsic and scale-dependent properties of CNTs. Heat transfer within an individual single-walled carbon nanotube (SWNT) is different from that in other carbon structures (graphenes, graphites) due to the periodic boundary conditions along the CNT circumference.[5,6] Estimated SWNT thermal conductivity (300−3000 W/(m·K) at room temperature) and the length dependence of thermal conductivity and ballistic-diffusive features of heat conduction have been predicted by molecular dynamics (MD) models.[7−10] The effective thermal conductivities of SWNT[11] and multi-walled carbon nanotube (MWNT)[12] bundles were experimentally measured[13−18] to show large variation and deviation from the calculated values. These differences possibly originate from the type of CNTs (quality, defects, diameter, length, chilarity, and number of walls), CNT morphology (dispersion, inter-CNT interactions such as roping, alignment, waviness, CNT-CNT contacts, etc.), interwall interactions, and phonon transport inside CNTs (mean free path). Experimental control of these important parameters is not possible at the current time (e.g., CNT−CNT contact is not a controllable experimental variable), and therefore computational models can best elucidate the effects of these parameters.

Models such as the modified effective medium theory (EMT),[19,20] which is limited to simple, noninteracting geometries, have been undertaken to quantify some of these factors on thermal transport solely with MD[21,22] or Monte Carlo[23] simulations. A different and meshless approach, based on a random walk algorithm, has been developed by introducing the thermal boundary resistance (TBR) at the CNT−matrix interface[24,25] and using Monte Carlo based models[26,27] to predict the thermal conductivities of MWNT−[28] and SWNT−polymer nanocomposites (PNCs).[29] This method simulates the quasi-phonon particle at an intermediate physical scale that allows CNT morphology, anisotropy, and interfacial CNT−CNT or CNT−matrix effects[23,28,29] to be considered in an efficient computational scheme. The first simulation results have been validated by comparison with experimental data of randomly oriented SWNT−PNCs.[30,31] Duong et al.[23] predicted the effective thermal conductivities of the PNCs having CNTs randomly

* Corresponding author: e-mail, hmd32@cam.ac.uk; telephone, +44 (0) 1223 334335.
† Massachusetts Institute of Technology.
‡ University of Cambridge.
§ National University of Singapore.
|| The University of Oklahoma.
⊥ The University of Tokyo.

10.1021/jp102138c

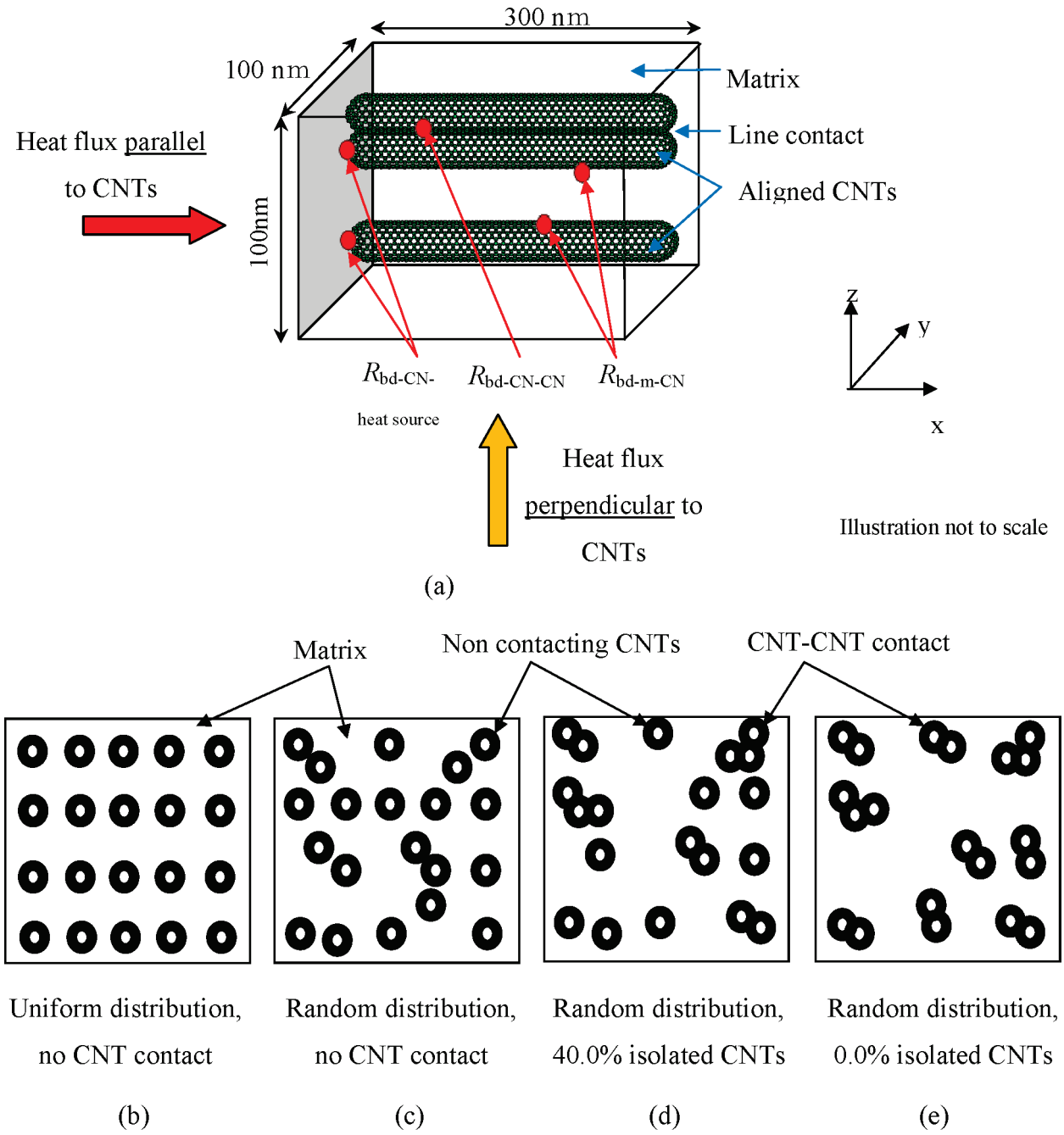

Figure 1. This figure is irrespective of SWNTs and MWNTs, it covers both. Parameters used in this study: (a) Schematic drawing of CNTs with different interfaces and therefore TBRs, and a top ($y-z$ plane) view of 20 CNTs (b) uniform CNT distribution (square packing); (c) 100.0% CNT isolation degree (no contact); (d) random distribution and random contact (40.0% isolated CNTs); and (e) random distribution with 0.0% isolated CNTs dispersed in the CNT−epoxy composite at 20 vol % of the CNTs, respectively.

dispersed with and without CNT contact under a wide range of CNT volume fractions. However, only a single large value of the CNT−CNT TBR was used, and the possibility of better CNT−CNT interaction that can decrease the CNT−CNT TBR has not been considered. In the present paper, the simulation methodology is applied to explore CNT−CNT interactions more appropriately, particularly the effects of a wide range of the CNT−CNT TBRs, CNT isolation degree, and the distribution of aligned CNTs in aligned-CNT PNCs. Anisotropic (along the CNTs vs perpendicular to the CNT alignment axis) heat conduction is quantified and the effects of morphology and CNT−CNT contact on anisotropy ratios are determined. Comparison of the simulated results with experiments can assist experimentalists in selecting an appropriate fabrication process to address CNT contact and agglomeration. The results can also be used with a representative volume element (RVE) approach to design optimized heat conduction materials using CNTs,[37] including complex 3D hybrid fiber−matrix composites reinforced with aligned CNTs currently under development.[38−40]

2. Approach

Different interfaces (and TBRs) such as CNT−CNT, CNT−heat source, and CNT−matrix TBRs are shown in Figure 1a. TBR values have not been directly measured, but the range of values reported in the literature from experiments and modeling is summarized here to establish a range for the simulations. Maruyama et al.[21] applied MD simulations to

TABLE 1: Material Properties and Parameters Used in the Simulations[a]

	SWNT	MWNT
	Geometry	
computational cell size (nm^3)	$300 \times 100 \times 100$	$300 \times 100 \times 100$
CNT diameter (nm)	2.4	8.0
CNT length (nm)	300	300
CNT volume fraction (%)	1, 8, 20	1, 8, 20
number of CNTs in a cell	22, 179, 448	2,[b] 16, 40
	Thermal Property	
thermal boundary resistance at the CNT−matrix interface, $R_{bd-m-CN}$ ($\times 10^{-8}$ m^2 K/W)[c]	174, 4.36, 0.44, 0.17, 0.09	174, 4.36, 0.44, 0.17, 0.09
thermal boundary resistance at the CNT−CNT interface, $R_{bd-CN-CN}$ ($\times 10^{-8}$ m^2 K/W)[c]	24.8, 8.67, 1.73	24.8, 8.67, 1.73
probability for phonon transmission from matrix to CNT, f_{m-CN}	0.0005, 0.02, 0.20, 0.50, 1.00	0.0005, 0.02, 0.20, 0.50, 1.00
probability for phonon transmission from CNT to CNT, f_{CN-CN}	0.0024, 0.2000, 1.0000	0.0024, 0.2000, 1.0000
thermal conductivity of matrix, K_m (W/(m·K))	0.2	0.2
thermal equilibrium factor, C_f		
without CNT−CNT contacts	0.248	0.319
with CNT−CNT contacts	0.230	0.295
	Simulation Conditions	
number of walkers	90000	90000
time increment, Δt (ps)	0.25	0.25
heat flux direction	parallel and perpendicular to the CNT axis	
CNT−CNT contacts	set by placing the aligned CNTs randomly in the volume and if they overlap, the CNTs are placed in contact	

[a] This set of simulation conditions includes the database developed in ref 23, augmented with conditions specifically designed to explore the effects of the CNT−CNT thermal boundary resistance. [b] Two MWNTs are forced to be in contact in this case rather than a random assignment. [c] Thermal boundary resistance R_{bd} is calculated from eq 2; epoxy specific heat is 0.97 J/(g·K);[50] epoxy density is 1.97 g/cm^3;[50] sound velocity in epoxy is 2400 m/s;[51] SWNT density is 1.30 g/cm^3;[52] sound velocity in SWNTs is 8000 m/s;[53] and SWNT specific heat is 0.625 J/(g·K).[54] The same f_{CN-CN} is assumed for the MWNTs due to unavailable values in the literature to calculate f_{CN-CN} using eq 2.

estimate the TBR between SWNTs in a bundle. Zhong et al.[22] reported systematic MD studies of the effect of contact morphology on the TBR. The reported values of the CNT−CNT TBRs range between 8×10^{-8} and 25×10^{-8} m^2 K/W. This value range is slightly higher than reported CNT−polymer matrix TBRs (i.e., 1.0×10^{-8} m^2 K/W for SWNT−PMMA[29] and 4.3×10^{-8} m^2 K/W for SWNT−epoxy[29]), and it is also higher than the range of SWNT−matrix TBRs ($(0.1-4.4) \times 10^{-8}$ m^2 K/W) used for simulations in the previous work of Duong et al.[23] In this work (see Figure 1a), CNT line contact is assumed and the CNT−heat source TBR is assumed to be equal to the CNT−matrix TBR for simplicity. As the CNT−CNT TBR can be decreased by functionalizing the CNTs to achieve better contact between the CNTs, this work employs a wider CNT−CNT TBR range, which includes a CNT−CNT TBR lower than that of CNT−matrix TBR (Tables 1 and 2). Several authors[32−34] have predicted that the wavy shape and spatial agglomeration of CNTs have a large (detrimental) influence on the effective elastic moduli of CNT-reinforced PNCs, and recent work addresses CNT waviness and distribution on nonmechanical physical properties such as electrical conduction.[35,36] The wavy CNT morphology also results in intermittent CNT−CNT contact. This morphology effect on effective thermal transport is studied here by considering the limiting case of fully contacting straight CNTs, leaving the case of wavy and intermittent CNT contact for future work. Through the CNT isolation degree study (Table 3) in this work, the model allows consideration of spatial CNT agglomeration, a significant parameter that helps to evaluate and select appropriate matrix materials and fabrication procedures in PNC design. CNT isolation degree is defined as the ratio of the number of isolated CNTs to the total number of CNTs in a computational cell (see illustrations in Figure 1).

3. Simulation Algorithm

The computational domain ($300 \times 100 \times 100$ nm^3) contains CNTs organized in the polymer matrix, collimated, and extended from one end of the computational domain to the other. In most of the cases, the locations of the CNTs were randomly assigned (Figures 1c and 1d) and/or forced to be in contact (see Figure 1e). The computational cell is heated from one surface (the $x = 0$ plane in Figure 1a) with the release of 90000 hot walkers distributed uniformly (square packing) on that surface at every time step. Walkers are therefore dropped into either the matrix or the CNTs depending on location of the CNTs, i.e., PNC morphology. The walkers, which are carrying heat, travel in the computational cell until steady state is achieved. At each time step, the walkers move through the matrix material by Brownian motion[41] with random jumps (σ)

$$\sigma = \sqrt{2D_m \Delta t} \tag{1}$$

where D_m is the thermal diffusivity of the matrix material and Δt is the time increment.

Once a walker in the matrix reaches the interface between the matrix and a CNT, the walker will move into the CNT with a probability f_{m-CN}, which represents the TBR of the interface, and will stay at the previous position in the matrix with a probability $(1 - f_{m-CN})$. According to the acoustic mismatch theory,[42] f_{m-CN} is given by

$$f_{i\text{-}CN} = \frac{4}{\rho_i C_i \nu_i R_{bdi}} \tag{2}$$

where i can be any material in contact with the CNT seen as the matrix f_{m-CN}, ρ is the density, C is the specific heat, ν is the

TABLE 2: Summary of CNT−CNT TBR Effects on Simulated Normalized Thermal Conductivities (K_{eff}/K_m) of SWNT− and MWNT−PNCs for 40% Isolated Randomly Distributed CNTs, Randomly Distributed Isolated CNTs (No CNT−CNT Contact), and CNTs with 100% Isolated Uniformly Distributed (Square Packing)[a]

	K_{eff}/K_m																				
	CNT−CNT contact random CNT distribution													no CNT−CNT contact, random CNT distribution					no CNT−CNT contact, uniform CNT distribution				
	$R_{bd-CN-CN}$ [$\times 10^{-8}$ m^2 K/W] (f_{CN-CN})																				
	24.8 (0.0024)				8.67 (0.2000)				1.73 (1.0000)												
	$R_{bd-m-CN}$ [$\times 10^{-8}$ m^2 K/W] (f_{m-CN})				$R_{bd-m-CN}$ [$\times 10^{-8}$ m^2 K/W] (f_{m-CN})				$R_{bd-m-CN}$ [$\times 10^{-8}$ m^2 K/W] (f_{m-CN})					$R_{bd-m-CN}$ [$\times 10^{-8}$ m^2 K/W] (f_{m-CN})					$R_{bd-m-CN}$ [$\times 10^{-8}$ m^2 K/W] (f_{m-CN})				
vol % (no. of CNTs)	4.36 (0.02)	0.44 (0.20)	0.17 (0.50)	0.09 (1.00)	4.36 (0.02)	0.44 (0.20)	0.17 (0.50)	0.09 (1.00)	174 (5×10^{-4})	4.36 (0.02)	0.44 (0.20)	0.17 (0.50)	0.09 (1.00)	174 (5×10^{-4})	4.36 (0.02)	0.44 (0.20)	0.17 (0.50)	0.09 (1.00)	174 (5×10)	4.36 (0.02)	0.44 (0.20)	0.17 (0.50)	0.09 (1.00)
SWNTs‖HeatFlux																					
1.0 (22)	1.59	3.30	4.22	4.83	1.62	3.44	4.48	5.42	1.03	1.66	3.59	4.71	5.46	1.02	1.64	3.65	4.85	5.60		1.65	3.75	5.02	5.96
8.0 (179)	3.44	9.52	14.1	17.8	3.97	13.2	21.3	28.3	1.21	4.32	15.1	25.3	34.5	1.15	4.20	15.1	26.1	37.1		4.38	17.4	31.1	44.6
20.0 (448)	4.89	15.3	24.7	34.8	6.63	28.1	53.3	80.8	1.57	7.79	35.2	70.9	112	1.36	7.39	36.6	79.4	132		8.13	48.6	116	209
SWNTs⊥Heat Flux																					
1.0 (22)	0.98	0.99	1.00	1.01	0.98	0.99	1.00	1.01	0.97	0.98	0.99	1.00	1.01	0.96	0.97	0.98	0.99	1.01		0.98	0.99	1.00	1.01
8.0 (179)	0.83	0.90	0.98	1.07	0.84	0.92	1.02	1.12	0.82	0.84	0.95	1.06	1.17	0.79	0.83	0.89	0.97	1.07		0.82	0.89	0.98	1.07
20.0 (448)	0.67	0.78	0.95	1.21	0.74	0.89	1.07	1.31	0.68	0.80	1.05	1.24	1.46	0.59	0.65	0.76	0.93	1.20		0.52	0.64	0.85	1.22
MWNTs‖ Heat Flux																					
1.0 (2)	1.19	1.63	1.77	1.85	1.20	1.67	1.84	1.94	1.02	1.22	1.67	1.86	1.97	1.01	1.23	1.91	2.21	2.38		1.24	1.92	2.21	2.39
8.0 (16)	2.24	5.09	6.76	8.13	2.44	5.96	8.17	9.89	1.08	2.56	6.38	8.83	10.7	1.05	2.52	6.65	9.49	11.7		2.56	6.93	9.94	12.2
20.0 (40)	3.34	9.24	13.7	17.8	4.10	13.0	20.1	26.2	1.25	4.47	14.5	22.7	30.4	1.15	4.35	16.0	26.9	38.1		4.62	18.4	30.8	42.3
MWNTs⊥Heat Flux																					
1.0 (2)	0.99	1.00	1.01	1.02	0.99	1.01	1.02	1.02	0.98	0.99	1.01	1.01	1.02	0.97	0.98	0.99	1.01	1.01		0.99	1.00	1.01	1.02
8.0 (16)	0.87	1.00	1.10	1.17	0.88	1.01	1.10	1.16	0.87	0.89	1.01	1.10	1.16	0.85	0.87	0.99	1.07	1.13		0.87	1.00	1.08	1.14
20.0 (40)	0.73	1.02	1.26	1.48	0.87	1.53	1.97	2.31	0.77	0.89	1.64	2.18	2.62	0.67	0.70	0.98	1.21	1.37		0.67	0.97	1.19	1.36

[a] Data corresponding to the case of isolated CNTs and random CNT distribution were obtained from the database developed in ref 23.

TABLE 3: Effects of CNT Isolation Degree on Thermal Conductivities of the 20 vol % SWNT− and MWNT−PNCs with Highest CNT−CNT TBR and Randomly Distributed CNTs[a]

	K_{eff}/K_m							
	$R_{bd-CN-CN} = 24.8 \times 10^{-8}$ m^2 K/W ($f_{CN-CN} = 0.0024$)							
CNT isolation degree (%)	$R_{bd-m-CN}$ [$\times 10^{-8}$ m^2 K/W] (f_{m-CN})				$R_{bd-m-CN}$ [$\times 10^{-8}$ m^2 K/W] (f_{m-CN})			
	4.36 (0.02)	0.44 (0.20)	0.17 (0.50)	0.09 (1.00)	4.36 (0.02)	0.44 (0.20)	0.17 (0.50)	0.09 (1.00)
	SWNTs ∥ Heat Flux				SWNTs ⊥ Heat Flux			
100.0	7.39	36.6	79.4	132	0.65	0.76	0.93	1.20
67.9	6.51	24.9	44.9	68.3	0.66	0.77	0.94	1.21
32.5	4.89	15.3	24.7	34.8	0.67	0.78	0.95	1.21
	MWNTs ∥ Heat Flux				MWNTs ⊥ Heat Flux			
100.0	4.35	16.0	26.9	38.1	0.70	0.97	1.19	1.36
67.5	3.40	9.95	15.2	20.1	0.71	0.99	1.22	1.41
40.0	3.34	9.24	13.7	17.8	0.73	1.02	1.26	1.48
0.00	3.24	8.66	12.4	15.4	1.03	1.40	1.64	1.87

[a] Data corresponding to the case of isolated CNTs and random CNT contacts were obtained from the database developed in ref 23.

velocity of sound in the matrix material, and R_{bd} is the thermal boundary resistance. A walker inside a CNT distributes randomly to give a uniform distribution due to the high CNT thermal conductivity compared to that of the matrix. The walker will redistribute randomly within the same CNT with a probability $(1 - f_{CN-m} - f_{CN-CN})$ at the end of a time step or will distribute randomly in other CNTs in contact with the previous CNT with a probability f_{CN-CN} or will cross into the matrix phase with a probability f_{CN-m}. In this latter case, the walker moves first to a point on the surface of the CNT and then moves into the matrix with a statistical jump whose magnitude takes values from a normal distribution that has a standard deviation given by eq 1 above. The probability f_{CN-m} is calculated by[23]

$$V_{CN} f_{CN\text{-}m} = C_f \sigma A_{CN} f_{m\text{-}CN} \quad (3)$$

where A_{CN} and V_{CN} are the surface area and the volume of a CNT, respectively, and C_f is a thermal equilibrium factor depending on the reinforcement (SWNT and MWNT) size and shape.[23,28,29]

The temperature distribution is calculated from the number of walkers found in discretized bins in the domain after steady state is reached. These bins are used only to count walkers for this calculation. In order to make the calculation of the effective thermal conductivity more rapid and straightforward, heat transfer with constant heat flux through a domain enclosed between a hot and a cold plane is studied. In this case, the two opposite planes release hot or cold (carrying negative energy)[43] walkers, respectively. The input simulation parameters are summarized in Table 1. Simulation runs are conducted with CNT−matrix and CNT−CNT TBRs, CNT orientation related to heat flux, and volume fraction of SWNTs and MWNTs in epoxy. Further details of the random walk algorithm and assumptions can be found in previous studies.[23,28,29]

4. Simulation Results and Discussion

Simulation results are presented here on the influences of CNT−CNT TBRs, CNT isolation degree, and CNT distribution on the effective thermal conductivities of the SWNT− and MWNT−PNCs. The data presented herein includes results from the simulations presented in ref 23, augmented with new simulations, in order to develop a complete picture of the effects of these parameters. CNT−CNT contact is a common occurrence as CNTs form bundles and also when SWNTs and MWNTs are grown into forests or spun into macroscopic fibers, which are wavy and in contact.[44] As mentioned already, the results presented here consider collimated CNTs only. The SWNT and MWNT diameters used in the simulations were 2.4 and 8.0 nm, respectively, corresponding to typical CNTs synthesized in the authors' groups.[37−40,45,46] The number of CNTs in the computational cell varied from 22 to 448 (SWNTs) and from 2 to 40 (MWNTs), depending on the volume fractions of CNTs in the polymer matrix (1−20 vol %). The simulations were conducted with different CNT−matrix TBRs ($R_{bd-m-CN}$ = 0.09, 0.17, 0.44, 4.36, 174 [$\times 10^{-8}$ m^2 K/W], i.e., probability f_{m-CN} = 1.0000, 0.5000, 0.2000, 0.0200, 0.0005, respectively); with different CNT−CNT TBRs, $R_{bd-CN-CN}$ ($R_{bd-CN-CN}$ = 1.73, 8.67, 24.8 [$\times 10^{-8}$ m^2 K/W] (f_{CN-CN} = 1.0000, 0.2000, 0.0024, respectively) falling within the wider range (10^{-8} to 10^{-7} m^2 K/W) of TBR values considered in the literature).[47] Different CNT volume fractions (1, 8, and 20 vol %) are considered, and the matrix used for the simulations was epoxy having thermal conductivity $K_m = K_{epoxy}$ = 0.2 W/(m·K).[29]

4.1. Effects of CNT−CNT TBR on the Effective Thermal Conductivities of PNCs. In both directions (heat flux is parallel and perpendicular to the CNT axis in Figure 2) of MWNT−PNCs, with the CNT volume fraction and the CNT−CNT TBR fixed, the normalized thermal conductivity of the PNC (K_{eff}/K_m) of CNT−PNCs having 40% isolated CNTs increases as the CNT−matrix TBR is reduced, as expected. CNT isolation degree and the associated TBR also have a strong effect on the effective thermal conductivity, again with higher conductivity associated with lower CNT−CNT TBR. CNT−CNT contact has a stronger influence on the effective thermal conductivity along the CNT axis (parallel direction) when the CNT−matrix TBR is relatively low with increasing CNT−CNT TBR. This is explained because heat remains in the matrix longer due to the high CNT−CNT TBR and therefore less phonons enter the high conductivity CNTs. At 20 vol % of CNTs, the CNT−matrix and CNT−CNT TBRs dramatically affect the effective thermal conductivities of the CNT−PNCs. The CNT−PNC having 20 vol % of CNTs reaches maximum effective parallel thermal conductivity ($K_{eff\text{-}maximum}/K_m$ = 30.4, or K_{eff} = 6.08 W/(m·K)) in Figure 2a at the lowest CNT−matrix TBR (0.09×10^{-8} m^2 K/W) and lowest CNT−CNT TBR (1.73×10^{-8} m^2 K/W). For the PNCs having CNTs perpendicular to the heat flux (Figure 2b), the enhancement of the effective thermal conductivity can be reversed depending on the CNT−matrix TBR and a critical CNT−matrix TBR can be defined (e.g., $\sim 0.7 \times 10^{-8}$ m^2 K/W for 1 and 8 vol %). If the CNT−matrix TBR is smaller than

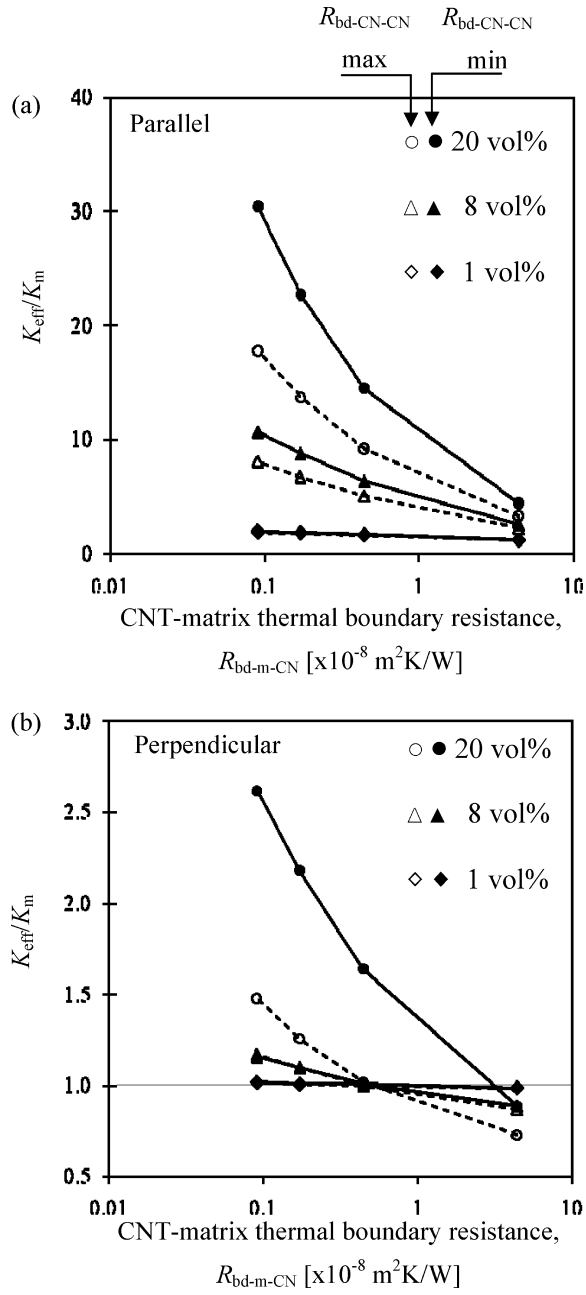

Figure 2. These plots consider the effects of high and low CNT−CNT TBR with 40% isolated MWNTs. Comparison of effective thermal conductivity of MWNT−epoxy having the CNT−CNT contact with different CNT−CNT TBRs, $R_{bd-CN-CN} = 1.73 \times 10^{-8}$ m^2 K/W (solid dots) and 24.8×10^{-8} m^2 K/W (open dots) as a function of thermal boundary resistance with different volume fractions of CNTs and the CNTs oriented (a) parallel and (b) perpendicular to the heat flux.

the critical CNT−matrix TBR, the effective perpendicular thermal conductivity of the PNCs is enhanced, with the usual trends of higher conductivity at higher volume fraction of CNTs and lower CNT−matrix TBRs. Above the critical CNT−matrix TBR, the effective thermal conductivity in the perpendicular direction is reduced and the trends are reverse. This is because at high CNT−matrix TBRs, the CNTs are effectively removed from thermal transport and act like excluded volume, rather than high-conductivity additions to the matrix. At 20 vol %, the effective perpendicular thermal conductivity is reduced (lower than thermal conductivity of epoxy matrix) and reaches a minimum ($K_{eff\text{-}minimum} = 0.77 \times K_{epoxy} \simeq 0.15$ W/(m·K)) with highest CNT−matrix TBR (4.36×10^{-8} m^2 K/W) and highest CNT−CNT TBR (24.8×10^{-8} m^2 K/W). Note that no critical matrix−CNT TBR is identified for heat conduction in the parallel direction, although the effect of CNT−CNT contact can still be quite significant (but not reverse trends).

Table 2 summarizes analyses for SWNT- and MWNT-PNCs with varying volume fraction, having varying CNT−matrix and CNT−CNT TBRs with different CNT arrangements (uniform square packing and random distribution with and without contact). In Table 2, for heat flux parallel to the axis of the CNTs, at the point for 20 vol % and for minimum CNT−matrix TBR, there is a ×1.2, ×1.6, and ×3.8 decrease in effective thermal conductivity with increasing CNT−CNT TBR when SWNT−SWNT contact is considered. This is because the phonons have less interfacial surface to cross into the high-conductivity CNTs from the matrix due to CNT grouping when they are in contact. Over the wider range of CNT−CNT TBR values (see Table 2) than considered previously, the thermal conductivity enhancement of SWNTs in PNCs with increased CNT volume fraction is greater, and less, than MWNTs for the case of parallel and perpendicular heat conduction, respectively.

In Figure 3a, when the CNT−CNT TBR ($R_{bd-CN-CN} = 1.73 \times 10^{-8}$ m^2 K/W) is smaller than the CNT−matrix TBRs ($R_{bd-m-CN} = 4.36, 174 \times 10^{-8}$ m^2 K/W), the heat transport of the walkers through the CNT−CNT contacts becomes more significant than through the CNT−matrix−CNT contacts. The walkers have greater likelihood to cross into the adjacent CNTs in contact resulting in an increase in the effective thermal conductivity of the PNCs. Therefore, the effective thermal conductivity of the PNCs having CNT−CNT contact with a very low CNT−CNT TBR is larger than that without CNT−CNT contact, when CNTs are parallel to the heat flux. This result is very interesting and helpful for experimental work and for applications. Instead of increasing the CNT volume fraction to enhance the effective thermal conductivity of the CNT−PNCs, the thermal conductivity can be enhanced by improving the CNT−CNT contact, possibly through CNT functionalization. Recent experimental work[48] has reported that the thermal conductivity of SWNT−polystyrene composites does not increase with the CNT volume fraction as much as predicted at higher volume fractions. Such difference might very well be due to the increase of the SWNT−SWNT contact points and higher values or CNT−CNT TBRs relative to the CNT−matrix TBR. For the perpendicular case (Figure 3b), the effective thermal conductivities of the CNT−PNCs without CNT contact are greater than those with the CNT−CNT contact. Below the critical point, the trend reverses as discussed previously due to the relative contributions of CNT−CNT TBR vs CNT−matrix TBR.

4.2. Effects of CNT Isolation Degree on the Thermal Conductivity of the PNCs. Here, we consider the effect of CNT−CNT contact degree by controlling (forcing) different degrees of CNT contact considering randomly dispersed CNTs as summarized in Table 3. Thermal conduction anisotropy ratios ($K_{eff\text{-}parallel}/K_{eff\text{-}perpendicular}$) of MWNT−epoxy composites with and without CNT−CNT contact (largest CNT−CNT TBR, $R_{bd-CN-CN} = 24.8 \times 10^{-8}$ m^2 K/W) are compared in Figure 4. CNT contact has a significant effect on the anisotropy ratio at high CNT loading, and low CNT−matrix TBR for this case (Figure 4) when the CNT−CNT TBR is very large (largest in the range considered in this work). In Table 2, with lower CNT−matrix TBR and higher CNT volume fraction, the reduction of $K_{eff\text{-}parallel}/K_{eff\text{-}perpendicular}$ ratios of the CNT−PNCs without and with the CNT−CNT contact is greater. At 20 vol % of MWNTs and the lowest CNT−matrix TBR (0.09×10^{-8}

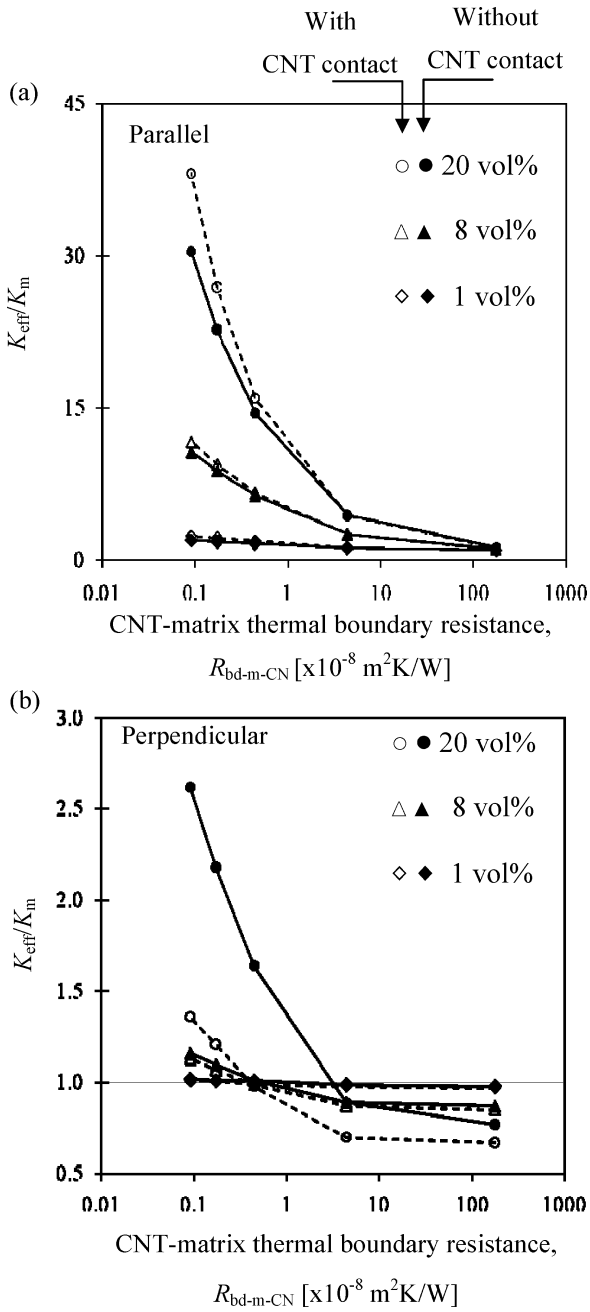

Figure 3. Comparison of effective thermal conductivity of MWNT−epoxy with (open dots, lowest CNT−CNT TBR, $R_{bd-CN-CN} = 1.73 \times 10^{-8}$ m^2 K/W) and without (solid dots) CNT−CNT contact as a function of CNT−matrix thermal boundary resistance with different volume fractions of CNTs and the CNTs oriented (a) parallel and (b) perpendicular to the heat flux.

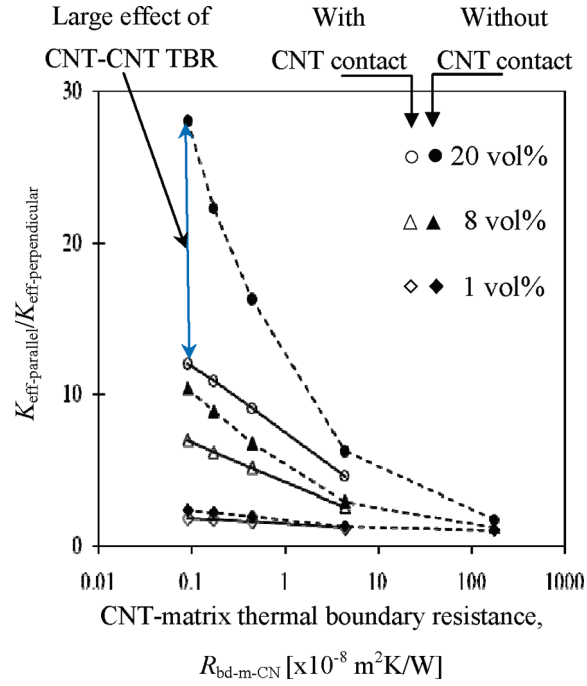

Figure 4. Comparison of thermal conductivity anisotropy ($K_{eff\text{-}parallel}/K_{eff\text{-}perpendicular}$) of MWNT−epoxy composites with (open dots, highest CNT−CNT TBR, $R_{bd-CN-CN} = 24.8 \times 10^{-8}$ m^2 K/W) and without (solid dots) the CNT−CNT contact as a function of CNT−TBR thermal boundary resistance with different volume fractions of CNTs.

m^2 K/W), the anisotropic heat conduction of the CNT−PNCs with the CNT−CNT contact decreases 2.3× compared with that without the CNT contact.

The simulation results of this part could be also very helpful interpreting experimental work. The effective thermal conductivities of the SWNT− and MWNT−PNCs having 20 vol % and the CNT−CNT TBR, $R_{bd-CN-CN} = 24.8 \times 10^{-8}$ m^2 K/W were studied over a wide range of the CNT isolation degree, from no isolated CNT (0.0%) to completely isolated CNTs (100.0%). Different isolation degree values (Table 3) are used to calculate the thermal conductivities of directional PNCs having the CNTs parallel and perpendicular to the heat flux. When the CNTs were randomly placed, 40.0% were in isolation for MWNTs and 32.5% for SWNTs. For the case of heat flux parallel to the CNT axis (Figure 5a and Table 3), the effective thermal conductivities of SWNT− and MWNT−PNCs decrease when the CNT isolation degree decreases. When the CNT−CNT TBR is larger than the CNT−matrix TBR, the more isolated CNTs provide larger effective thermal conductivity. The effective thermal conductivities of the CNT−PNCs are highest with completely isolated CNTs (100.0%) and lowest with 0.0% isolated CNTs. With the same CNT isolation degree and volume fraction, the effective thermal conductivities of the SWNT−PNCs are larger than those of the MWNT−PNCs due to the larger SWNT−matrix interfacial area. When CNT−matrix TBR increases, fewer walkers can cross into the CNTs to take advantage of the CNT high thermal conductivity. This makes the effective thermal conductivities of both SWNT− and MWNT−PNCs decrease with the same CNT isolation degree. In Figure 5a (parallel cases), with the same CNT volume faction and the CNT isolation degree, the effect on the effective thermal conductivities of the SWNT−PNCs is larger than those for MWNT−PNCs. This can be explained because the SWNT−matrix interface reduces significantly more than the MWNT−PNCs as the contact between CNTs increases.

For the case of heat flux perpendicular to the CNT axis (Figure 5b and Table 3), with same CNT isolation degree, effective thermal conductivities of MWNT−PNCs are larger than those of SWNT−PNCs. Again this is because walkers can travel faster along the MWNT diameter (8.0 nm), which is larger than the SWNT diameter (2.4 nm). The effective thermal conductivities of the SWNT− and MWNT−PNCs decrease when CNT−matrix TBRs increase. When decreasing the CNT isolation degree (100.0% down to 32.5% for SWNT−PNCs and 100.0% down to 40.0% for MWNT−PNCs), the effective thermal conductivities increase slightly (Table 3). Walkers can travel faster along the CNT diameter, cross the CNT−CNT interface, and move faster along next contacting CNT diameter.

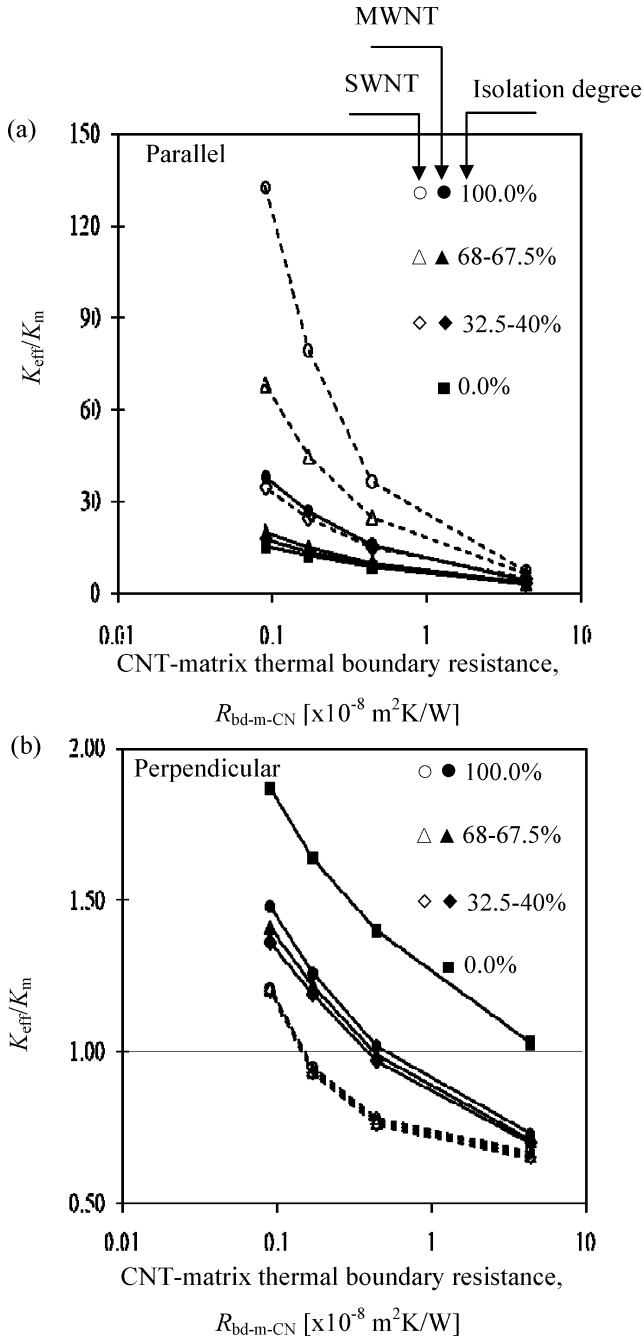

Figure 5. Comparison of effective thermal conductivity of MWNT−epoxy (solid dots and solid lines) and SWNT−epoxy (open dots and dashed lines) composites having 20 vol % and highest CNT−CNT TBR, $R_{bd-CN-CN} = 24.8 \times 10^{-8}$ m^2 K/W as a function of CNT−matrix thermal boundary resistance with different CNT isolation degree and the CNTs oriented (a) parallel and (b) perpendicular to the heat flux.

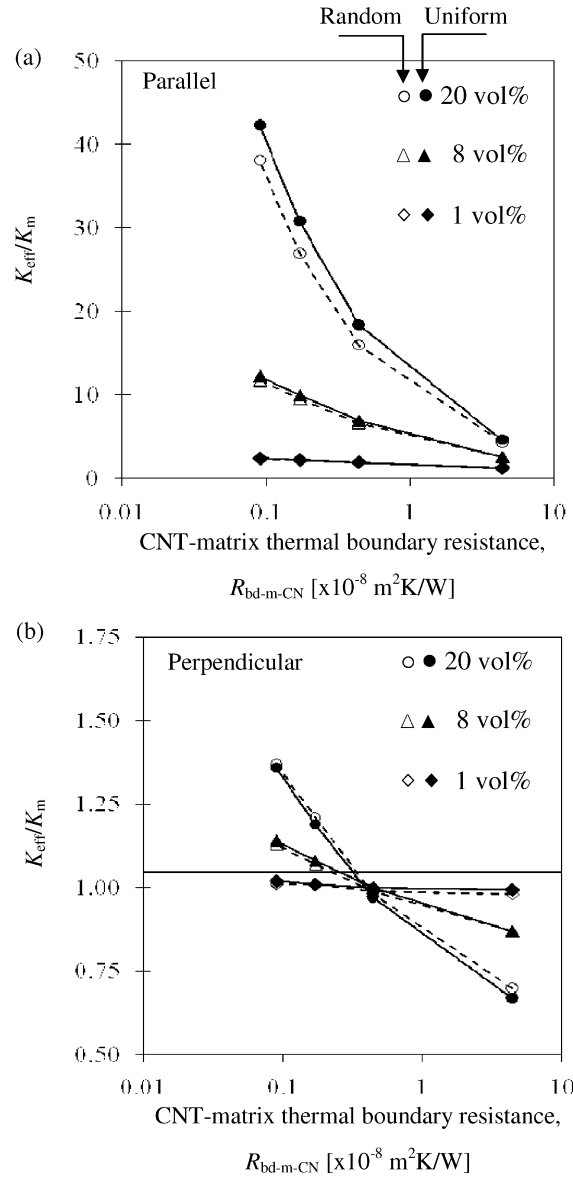

Figure 6. Comparison of effective thermal conductivity of MWNT−epoxy having no CNT−CNT contact with uniform CNT distribution (solid dots) and with random CNT distribution (open dots) effects with as a function of CNT−matrix thermal boundary resistance with different volume fractions of CNTs and the CNTs oriented (a) parallel and (b) perpendicular to the heat flux.

Especially with higher CNT volume fraction (20 vol %, Figure 5b), larger MWNT diameter, and the smallest CNT isolation degree (0.0%), walkers can move faster along the CNT radius and come out the computational cell quickly.

4.3. Effects of the CNT Distribution on the Thermal Conductivity of PNCs. Here we consider the effects of a uniform CNT distribution on the effective thermal conductivities of SWNT− and MWNT− PNCs without CNT−CNT contact (Table 2 and Figures 6 and 7). For uniformly distributed CNTs in the computational cell, the distance between two nearby CNTs in the same row or column was equal. As random distribution of the CNTs cannot preclude local CNT agglomeration in the PNCs, distributing the CNTs uniformly avoids this issue in the modeling.

For the CNTs parallel to the heat flux (Figure 6a), distribution (random vs uniform) has very little effect on effective thermal conductivities when CNT−CNT contact is not considered. These local CNT agglomerations prevent phonons from coming into the CNTs from the matrix. The effect of the CNT agglomeration increases with the high CNT volume fraction. In Figure 7a, with the same CNT volume fraction and the same CNT−matrix TBR, the thermal conductivities of the SWNT−PNCs are significantly larger than those of the MWNT−PNCs. In Table 2, this is shown for both CNT random and uniform distributions effects due to the larger interfacial area. At 20 vol % and the CNT−matrix TBR, $R_{bd-m-CN} = 0.09 \times 10^{-8}$ m^2 K/W, the uniform distribution effect can enhance ×1.6 and ×1.1 the effective parallel thermal conductivities of the SWNT− and MWNT−PNCs, respectively, relative to those with random distribution.

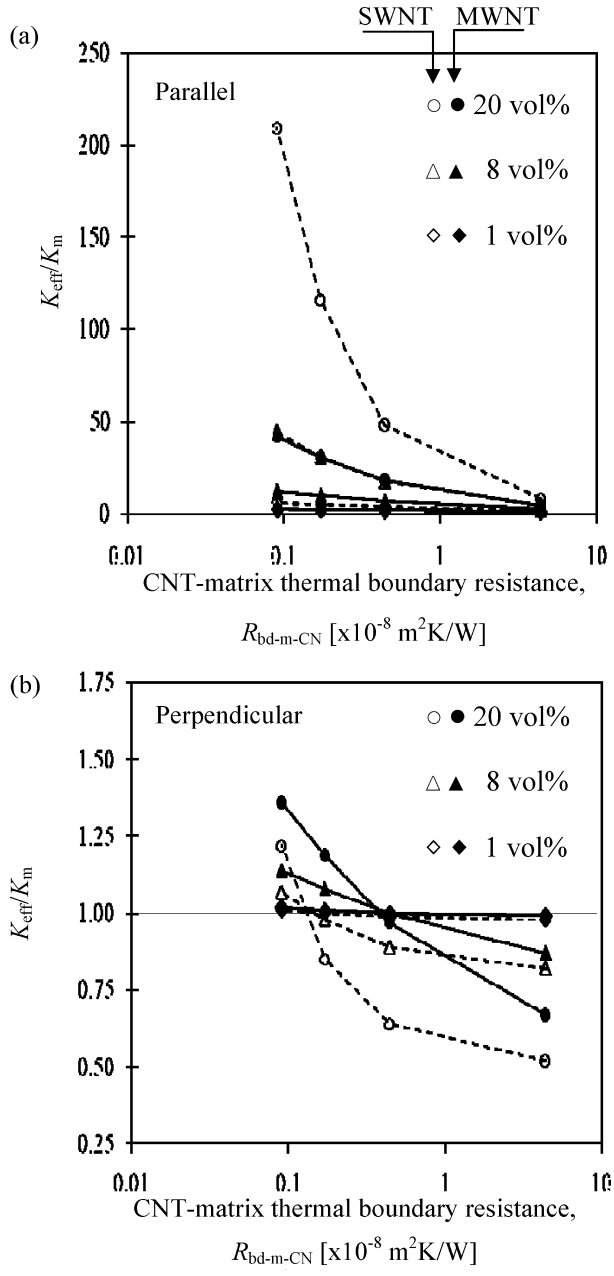

Figure 7. Comparison of effective thermal conductivity of MWNT−epoxy (solid dots, solid lines) and SWNT−epoxy (open dots and dashed lines) composites having no CNT−CNT contact with uniform CNT distribution as a function of CNT−matrix thermal boundary resistance with different volume fractions of CNTs and the CNTs oriented (a) parallel and (b) perpendicular to the heat flux.

For the CNTs perpendicular to the heat flux (Table 2 and Figure 6b), CNT distribution effects also do not play an important role on the thermal conductivities of MWNT−PNCs. This is true for SWNT−PNCs with low CNT volume fractions (1−8 vol %). For the SWNT−PNCs with CNT uniform distribution at the 20 vol % (Table 2), phonons have an increased chance of contacting a CNT, and there is a small effect. So with the higher CNT−matrix TBR, the CNTs block the phonons/walkers and make them travel slower in the matrix. Localized agglomeration can now have the opposite effect, i.e., when the SWNTs are agglomerized, the excluded area for heat transfer is smaller than when the SWNTs were well distributed in the PNCs. This makes the effective thermal conductivities of the CNT−PNCs with the uniform CNT distribution smaller. In Table 2 and Figure 7b, the ratio K_{eff}/K_m for MWNT− and SWNT−PNCs with the CNT uniform distribution at 20 vol % decreases below 1 when the CNT−matrix TBRs are larger than a critical CNT−matrix TBR (0.5×10^{-8} m^2 K/W for the MWNT−PNCs and 0.2×10^{-8} m^2 K/W for the SWNT−PNCs). With the same CNT−matrix TBR and the same CNT volume fraction, the thermal conductivities of the MWNT−PNCs are always larger than those of the SWNT−PNCs with the uniform CNT distribution due to larger MWNT diameter and less interfacial area.

5. Conclusions

A Monte Carlo model was applied to study the effects of aligned CNT array morphology on the effective thermal conductivities of the CNT−PNCs for a wide range of CNT−CNT and CNT−matrix TBRs, CNT distributions (random or uniform), CNT isolation degree, and CNT volume fractions. It was found that, when the CNT−CNT TBR is larger than the CNT−matrix TBR, the effect of increased nanotube contacts is detrimental to the effective thermal conductivity of PNCs with CNT acting as inclusions oriented in the direction of the heat flux. These detrimental effects are more pronounced for cases of high CNT volume fractions, perhaps explaining some confusing experimental results where thermal conductivity decreases as CNT volume fraction (but also contact) also increases. For the case of heat flux perpendicular to the direction of the axis of the CNTs, it was found that there exists a critical CNT−CNT TBR below which the effective conductivity of the CNT-PNCs falls below the thermal conductivity of the pure polymer. In this case, the effects of CNT−CNT contacts are more important for MWNTs rather than for SWNTs. The effects of agglomeration of CNTs, even when the CNTs are not in contact and there are no CNT−CNT TBR present, is also detrimental for the effective heat conductivity when the heat flux is parallel to the direction of the CNT axis. Since currently available calculations suggest that the CNT−CNT TBR is higher than the CNT−matrix TBR, it appears that there should be an effort to improve the quality of the CNT−CNT interface by reducing the thermal resistance at this interface, rather than focusing exclusively on increasing the volume fraction of the CNTs.

The current model does not take into account the CNT wavy shapes that give intermittent CNT−CNT contact. In addition, to validate the simulation results with experiments, future work should include exploration of a wider range of CNT−matrix interface resistance and quantification for different thermal interface materials like CNT−metal composites. The effects on TBRs of other molecules existing on the surface of synthesized CNTs and the possibility that the CNTs cause a local polymer interphase[34,49] different than the neat polymer should also be considered. Uneven CNTs topography due to the variation of CNT heights causing uneven contact with heat source[17] and contact in length direction for shorter CNTs than film thickness seems to be the critical problems for at least SWNTs.

Acknowledgment. This work was supported by Airbus S.A.S., Boeing, Embraer, Lockheed Martin, Saab AB, Spirit AeroSystems, Textron Inc., Composite Systems Technology, and TohoTenax through MIT's Nano-Engineered Composite Aerospace Structures (NECST) Consortium. This work was also supported by the TeraGrid under TG-CTS070050 and TG-CTS090017. Namiko Yamamoto acknowledges support from MIT's Linda and Richard Hardy (1958) Fellowship. Dimitrios Papavassiliou acknowledges support from the DoE-funded Carbon Nanotubes Technology Center (Award Register ER64239

0012293). Shigeo Maruyama acknowledges support from Grant-in-Aid for Scientific Research (19206024) from the Japan Society for the Promotion of Science, SCOPE (051403009) from the Ministry of Internal Affairs and Communications, and NEDO (Japan).

References and Notes

(1) Xu, J.; Fisher, T. S. *IEEE Trans. Compon. Packag. Technol.* **2006**, *29* (2), 261.
(2) Hu, X. J.; Panzer, M. A.; Goodson, K. E. *J. Heat Transfer* **2007**, *129* (1), 91.
(3) Ajayan, P. M.; Schadler, L. S.; Giannaris, C.; Rubio, A. *Adv. Mater.* **2000**, *12*, 750.
(4) Choi, S. U. S.; Zhang, Z. G.; Yu, W.; Lockwood, F. E.; Grulke, E. A. *Appl. Phys. Lett.* **2001**, *79*, 2252.
(5) Hone, J.; Whitney, M.; Piskoti, C.; Zettl, A. *Phys. Rev. B* **1999**, *59* (4), R2514.
(6) Dresselhaus, M. S.; Dresselhaus, G.; Avouris, Ph. *Carbon Nanotubes: Synthesis, Structure, Properties and Applications*; Springer: New York, 2001.
(7) Berger, S.; Kwon, Y. K.; Tomanek, D. *Phys. Rev. Lett.* **2000**, *84* (20), 4613.
(8) Maruyama, S. *Physics B* **2002**, *323*, 193.
(9) Yamamoto, T.; Konabe, S.; Shiomi, J.; Maruyama, S. *Appl. Phys. Express* **2009**, *2*, 095003.
(10) Mingo, N.; Broid, D. A. *Nano Lett.* **2005**, *5*, 1221.
(11) Pop, E.; Mann, D.; Wang, Q.; Goodson, K. E.; Dai, H. *Nano Lett.* **2006**, *6* (1), 96.
(12) Kim, P.; Shi, L.; Majumdar, A.; McEuen, P. L. *Phys. Rev. Lett.* **2001**, *87* (21), 215502.
(13) Hone, J.; Llaguno, M. C.; Nemes, N. M.; Johnson, A. T.; Fisher, J. E.; Walters, D. A.; Casavant, M. J.; Schmidt, J.; Smalley, R. E. *Appl. Phys. Lett.* **2000**, *77* (5), 666.
(14) Yi, W.; Lu, L.; Dian-lin, Z.; Pan, Z. W.; Xie, S. S. *Phys. Rev. B* **1999**, *59* (14), R9015.
(15) Shaikh, S.; Li, L.; Lafdi, K.; Huie, J. *Carbon* **2007**, *45* (13), 2608.
(16) Panzer, M. A.; Duong, H. M.; Okawa, J.; Shiomi, J.; Wardle, B. L.; Maruyama, S.; Goodson K. E. *Nano Lett.*, in press.
(17) Panzer, M. A.; Zhang, G.; Mann, D.; Hu, X.; Pop, E.; Dai, H.; Goodson, K. E. *J. Heat. Transfer* **2008**, *130*, 052401.
(18) Hone, J.; Whitney, M.; Piskoti, C.; Zettl, A. *Phys. Rev. B* **1999**, *59*, R2514.
(19) Nan, C. W.; Birringer, R.; Clarke, D. R.; Gleiter, H. *J. Appl. Phys.* **1997**, *81* (10), 6692–6699.
(20) Nan, C. W.; Liu, G.; Lin, Y.; Li, M. *Appl. Phys. Lett.* **2004**, *85* (16), 3549.
(21) Maruyama, S.; Igarashi, Y.; Taniguchi, Y.; Shiomi, J. *J. Therm. Sci. Technol.* **2006**, *1*, 138–148.
(22) Zhong, H.; Lukes, J. R. *Phys. Rev. B* **2006**, *74*, 125403.
(23) Duong, H. M.; Yamamoto, N.; Papavassilliou, D. V.; Maruyama, S.; Wardle, B. L. *Nanotechnology* **2009**, *20* (15), 155702.
(24) Kapitza, P. L. *J. Phys. (Moscow)* **1941**, *4*, 181.
(25) Maruyama, S.; Kimura, T. *Therm. Sci. Eng.* **1999**, *7* (1), 63.
(26) Tomadakis, M. M.; Sotirchos, S. V. *J. Chem. Phys.* **1993**, *98*, 616.
(27) Tomadakis, M. M.; Sotirchos, S. V. *J. Chem. Phys.* **1996**, *104*, 6893.
(28) Duong, H. M.; Papavassiliou, D. V.; Lee, L. L.; Mullen, K. J. *Appl. Phys. Lett.* **2005**, *87* (1), 013101.
(29) Duong, M. H.; Papavassiliou, D. V.; Mullen, J. K.; Maruyama, S. *Nanotechnology* **2008**, *19* (6), 065702.
(30) Bryning, M. B.; Milkie, D. E.; Kikkawa, J. M.; Yodh, A. G. *Appl. Phys. Lett.* **2005**, *87*, 161909.
(31) Du, F.; Guthy, C.; Kashiwagi, T.; Fischer, J. E.; Winey, K. I. *J. Polym. Sci., Part B: Polym. Phys.* **2006**, *44*, 1513.
(32) Cebeci, H.; Guzman de Villoria, R.; Hart, A. J.; Wardle, B. L. *Compos. Sci. Technol.* **2009**, *69*, 2649.
(33) Fisher, F. T.; Bradshaw, R. D.; Brinson, L. C. *Appl. Phys. Lett.* **2002**, *80*, 4647.
(34) Winey, K. I.; Vaia, R. A. *MRS Bull.* **2007**, *32* (4), 314.
(35) Li, C. Y.; Thostenson, E. T. *Compos. Sci. Technol.* **2008**, *68* (6), 1445.
(36) Dervishi, E.; Li, Z.; Saini, V.; Biris, A. R.; Lupu, D.; Trigwell, S.; Biris, A. S. *Mater. Res. Soc. Symp. Proc.* **2007**, *1018*, EE13−05.
(37) Wardle, B. L.; Saito, D. S.; Garcia, E. J.; Hart, A. J.; Guzman de Villoria, R. *Adv. Mater.* **2008**, *20*, 2707.
(38) Garcia, E. J.; Wardle, B. L.; Hart, A. J. *Composites, Part A* **2008**, *39*, 1065.
(39) Garcia, E. J.; Wardle, B. L.; Hart, A. J.; Yamamoto, N. *Compos. Sci. Technol.* **2008**, *68*, 2034.
(40) Garcia, E. J.; Hart, A. J.; Wardle, B. L.; Slocum, A. H. *Nanotechnology* **2007**, *18*, 165602.
(41) Einstein, A. *Ann. Phys.* **1905**, *17*, 549.
(42) Swartz, E. T.; Pohl, R. O. *Rev. Mod. Phys.* **1989**, *61*, 605.
(43) Sundqvist, B.; Sandberg, O.; Backstrom, G. *J. Phys. D: Appl. Phys.* **1977**, *10*, 1397.
(44) Einarsson, E.; Shiozawa, H.; Kramberger, C.; Ruemmeli, M. H.; Gruneis, A.; Pichler, T.; Maruyama, S. *J. Phys. Chem. C* **2007**, *111* (48), 17861.
(45) Murakami, Y.; Einarsson, E.; Edamura, T.; Maruyama, S. *Carbon* **2005**, *43*, 1664.
(46) Murakami, Y.; Chiashi, S.; Miyauchi, Y.; Hu, M.; Ogura, M.; Okubo, T.; Maruyama, S. *Chem. Phys. Lett.* **2004**, *385* (3−4), 298.
(47) Clancy, T. C.; Gate, T. S. *Polymer* **2006**, *47*, 5990.
(48) Peters, J. E.; Papavassiliou, D. V.; Grady, B. P. *Macromolecules* **2008**, *41* (20), 7274.
(49) Schadler, L. S.; Kumar, S. K.; Benicewicz, B. C.; Lewis, S. L.; Harton, S. E. *MRS Bull.* **2007**, *32*, 335.
(50) Yutopian, Thermal and Mechanical Properties of Epoxy. http://www.yutopian.com/Yuan/prop/Epoxy.html, 2008.
(51) Bick, A.; Dorfmueller, T. *NATO ASI Ser., Ser. C* **1989**, *291*, 389.
(52) Collins, P. G.; Phaedon, A. *Sci. Am.* **2000**, *67*, 68 and 69.
(53) Hone, J.; Whitney, M.; Zettl, A. *Syn. Met.* **1999**, *103*, 2499.
(54) Hepplestone, S. P.; Ciavarella, A. M.; Janke, C.; Srivastava, G. P. *Surf. Sci.* **2006**, *600*, 3633.

JP102138C